Indian Journal of Chemical Technology
Vol. 30, July 2023, pp. 483-491
DOI: 10.56042/ijct.v30i4.71226

Electrical impedance analysis of ZnO thin films for ammonia gas sensors

R.Mariappan[1]*, S. Dinagaran[2], P. Srinivasan[3] & S. Vijayakumar[4]

[1] Department of Physics, Adhiyamaan College of Engineering, Hosur - 635 109, Krishnagiri, Tamil Nadu, India

[2] University College of Engineering Thirukkuvalai, Thirukkuvalai - 610 204, Tamil Nadu, India

[3] Department of Physics, National Institute of Technology Silchar, Silchar, Assam, 788 010, India

[4] Government Arts College for Women, Karimangalam - 635 111, Dharmapuri, Tamil Nadu, India

*E-mail: mariappan.physics@adhiyamaan.in

Received 8 February 2023; accepted 2 April 2023

The electrical impedance analysis of the ZnO films has been performed using complex impedance spectroscopy in the frequency range from 100 Hz to 1 MHz with temperature change from 70 to 175°C. Combined impedance and modulus plots have been used to analyse the sample behaviour as a function of frequency at different temperatures. Temperature dependence of ac conductivity indicates that the electrical conduction in the material is a thermally activated process. The frequency dependence of the ac conduction activation energy is found to obey a mathematical formula. It is concluded that the conductivity mechanism in the ZnO sensor is controlled by surface reaction. The operating temperature of the ZnO gas sensor is 175°C. The impedance spectrum also exhibited a decreased semicircle radius as the ammonia concentration is increased from 50 to 500 ppm. In addition, the impedance spectrum also exhibited a decreased semicircle radius with the exposure time increase from 0 to 20 min thereafter slightly increased. Impedance spectroscopy analysis has shown that the resistance variation due to grain boundaries significantly contributed to the gas sensor characteristics.

Keywords: ZnO device, Impedance analysis, Ammonia sensor

The most widely studied area of solid state gas sensors is semiconducting oxides. Here the sensing element used have high surface-to-bulk ratio. Adsorption of a foreign species on a semiconducting surface gives rise to surface states and the electrical properties of these surfaces change as a result of adsorption and/or reaction[1,2]. This change in the semiconductor property is used to quantify the presence of specific reactive gas in the gaseous mixture. The phenomenon of a semi conductive film sensitive to the presence of gases was observed by Brattein and Bardeen[3] for Ge and later Heiland[4] and Bielanski[5] for metal oxides. Then the pioneering works of Seiyama[6] lead to the fabrication of first gas sensing device. This is because other semiconductors undergo irreversible chemical reactions forming stable oxides upon exposure to air at high temperatures, whereas metal oxides remain stable while interacting with oxygen at their surface.

In this study, electrical impedance and gas sensing properties of ZnO thin films deposited at different temperature by NSP technique was studied. Impedance spectra were recorded for air exposed films and ammonia (NH_3) gas exposed films at an operating temperature 175°C with a fixed 100 mV ac voltage. Sensor is continuously kept in the gaseous atmosphere while recording the impedance spectra for ZnO thin films. Spectra were also recorded for various exposure times by removing and introducing the sensors placed in the gaseous atmosphere. The deposition temperature, molar concentration, film thickness and the solvent used for synthesis were optimized as 400°C, 0.1 M, 342 nm and water, respectively, and the same were taken for the preparation of ZnO films.

Experimental Section

Fig. 1a shows the schematic diagram of the sensor device developed for the study. Sensor consists of ZnO layer deposited on top of ITO coated glass substrates using NSP technique. The ITO layer is to make sure that any change in resistance detected between the contacts originates from resistance variations in the film taken for the study. The contacts were made by sputtering of an electrode of Au through a shadow mask. The distance between the Au electrodes was about 2 mm and thickness ~225 nm. Prior to deposition, the surface was cleaned in acetone for 15 min followed by 15 min of ultrasonic treatment to remove organic contaminants. In DC reactive magnetron sputtering, the physical properties of the deposited films critically depend on sputtering parameters, such as, oxygen partial pressure,

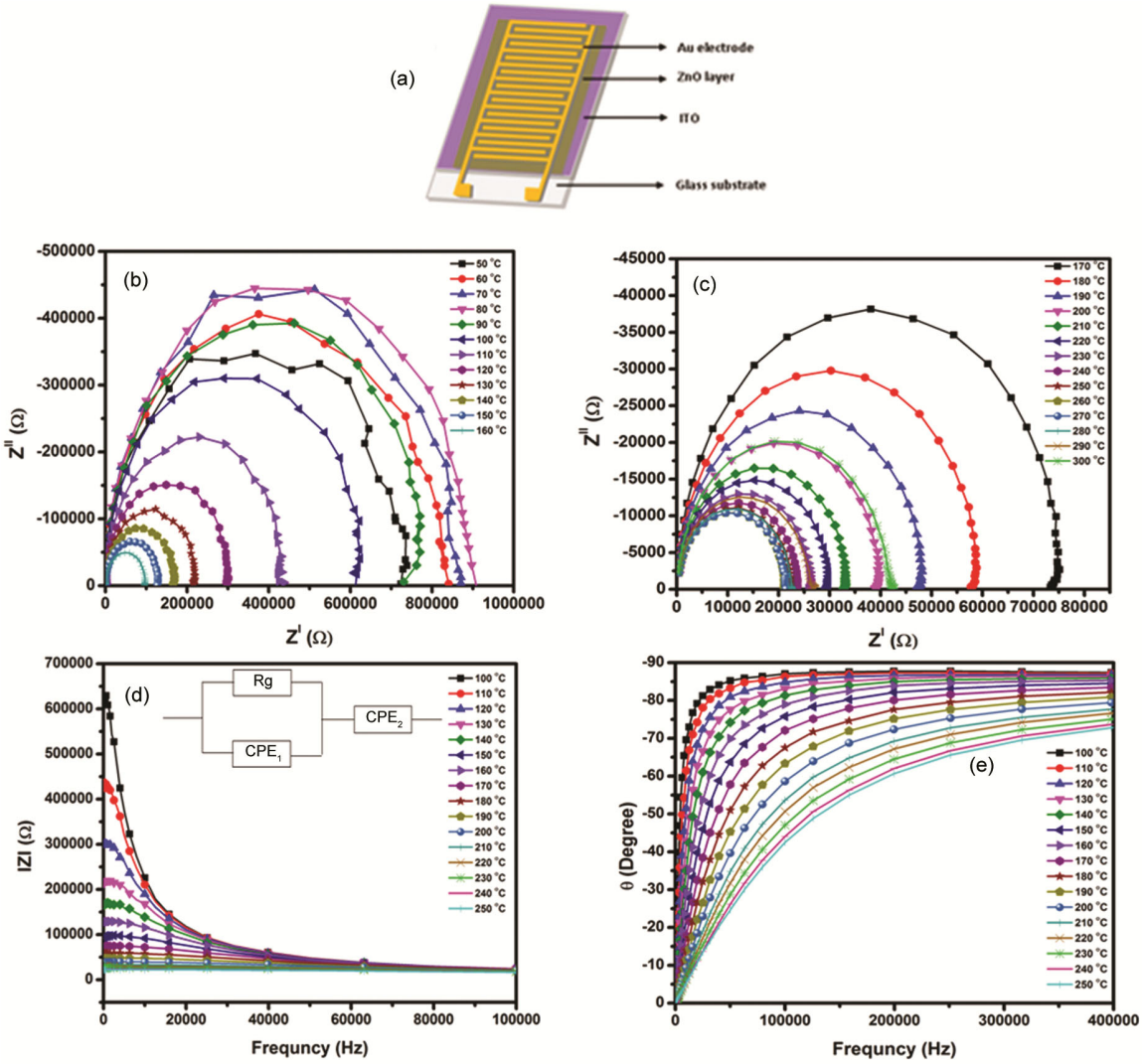

Fig. 1 — (a) Schematic diagram of ZnO sensor device, **(**b-c**)** Nyquist plots for ZnO device, **(**d**)** Modulus |Z| versus frequency of ZnO device (insert figure Equivalent circuits used to fit the impedance spectra for ZnO film), **(**e**)** Phase θ versus frequency of ZnO device

sputtering pressure, substrate temperature, sputtering power, and distance between the target and the substrate. When the sputtering chamber reached the required deposition pressure of 6.3×10^{-3} Torr, the DC power supply was turned on at 90 W to start the thin film deposition. The separation between the target and the substrate was approximately 1.5 cm. The O_2 to Ar gas flow ratios were maintained at 1:1 and film was deposited at 30 min after deposition, the film was annealed at 400°C for 1 h.

Results and Discussion

Electrical impedance analysis of ZnO device

Figs 1b-c shows the real ($Z^{/}$) and imaginary ($Z^{//}$) (Nyquist plots) parts of the in the complex impedance spectra and the corresponding equivalent circuits of ZnO thin films studied at temperatures changes from 50 to 300°C. At high frequency, the data show a semicircle indicating that the relaxation time of the bulk and the grain boundaries are close to each other. In the mid frequency range, a linear progress in the diffusion characteristics of ZnO is observed during insertion-desertion process. In the lowest frequency area, capacitive behaviour is observed showing the characteristic response of a finite blocked diffusion. Centre of the semicircle is localized below real axis is ascribed to constant phase element. Intersect on the real axis of the semicircle at low frequencies is ascribed to the total resistance. Conversely, the impedance response of grain dominates at high frequencies and resistances of grain (R_g) is deduced from the left intersect of the semicircle to real axis.

The intercept of semicircle to real axis ($Z^{/}$) at low frequency depicts the sum of resistance of grains and grain boundaries while an intercept at high frequency depicts the resistance of grain only. Grain boundary resistance decreases with temperature is due to the grain boundary effect which has assisted the lowering of the motion of charge carriers. The initial data of both resistance (R) and capacitance (C) were estimated manually at each temperature. R can be estimated from the diameter of the arc ($R=2Z^{/}$) (Figs 1b & 1c) and C can be found from the relation $\omega_{max} RC=1$.

The expressions, which relate the modulus |Z| and phase θ with frequency, are obtained from the real ($Z^{/}$) and imaginary part ($Z^{//}$) of the complex impedance of the above circuit equivalent as,

$$|Z| = \sqrt{Z^{/2} + Z^{//2}} \quad \text{... (1)}$$

$$\theta = \tan^{-1}\left(\frac{Z^{//}}{Z^{/}}\right) \quad \text{... (2)}$$

The resistance and capacitance associated with the solids could be estimated using impedance spectroscopy. The dependence of the modulus and phase versus frequency for the ZnO film are presented in Figs 1d and 1e, for selected temperature variation from 100 to 250°C.

Insert in Fig. 1d shows the equivalent circuit proposed to fit the impedance spectra of ZnO film which contains a series connection of resistor two capacitor (RC), connected in parallel, with the electrolyte resistance R_s indicating that there are two distinct layers of zinc oxide with electrical properties. At higher frequencies, the observed shapes are typical of relaxation mechanisms expressed by the constant phase elements (R_g-CPE_1) parallel circuits. At lower frequencies, electrode polarization effects transduced by constant-phase elements (CPE_2) are evidenced with a phase angle close to 85° indicating a near capacitive behavior for ZnO film. The phase shift reached a value around 75° of the ZnO film.

Temperature dependence of conductivity in ZnO device

Variation of resistivity and conductivity with function of temperature for the ZnO film with two frequencies 100 and 1000 Hz is shown in Fig. 2a. It is observed that (Fig. 2a) the total resistivity of the film decreases initially at the lower temperature region from 30 to 40°C. When the temperature increases from 50 to 70°C, the total resistivity of the film is found to be increased while conductivity slightly decreased. This increase in resistivity is attributed to the chemisorptions of oxygen on the film surface, causing a decrease in carrier concentration. This is consistent with the adsorption of oxygen on the surface of polycrystalline ZnO films as reported by other researchers[7-9]. However, in the present study four regions are very distinctly found and the resistivity change with temperature is shown in Fig. 2a and the result show good agreement with the reported by other researchers[10,11].

In region I, the decrease in total resistivity is attributed to the thermal excitation of electrons into the conduction band. The sharp increase in resistivity in region II is related to the vigorous oxygen absorption on the film surface. The resistivity in region III decreases again, probably due to the dominant thermal excitation of electrons and desorption of oxygen species.

It may also be related to the increase in carrier concentration resulting from the activation of deep donors arisen due to native defects such as interstitial zinc atoms and oxygen vacancies[12]. In region IV, the resistivity slightly increases again, probably due to the oxygen absorption on the film surface.

DC electrical conductivity of the ZnO film from complex impedance spectrum data was calculated as a function of temperature and the same is shown in Fig. 2a. The pattern indicates an increase in conductivity with increase of temperature and the electrical conduction in the ZnO film is a thermally activated transport process governed by Arrhenius type relation:

$$\sigma_{DC} T = \sigma_o \exp\left(-E_a / kT\right) \quad \text{... (3)}$$

where, T is the temperature, E_a is the activation energy for mobile ions, k represent the pre exponential factor. Since thermal excitation is the main cause of increase in electrical conductivity in regions I and IV the thermal activation energies were calculated from the plots of $\ln\sigma$ versus 1000/T as shown in Fig. 2b and their values are found to be 0.49 and 0.51 eV for 100 and 1000 Hz.

Electrical conduction mechanism

The ac method is an easy procedure for measuring the electrical conductivity of a film because at low frequencies the conductivity dependence can be expressed by the so called Jonscher power law[13],

$$\sigma^{/}(low\ freq.) = \sigma_{dc} + A\omega^{s} \qquad s < 1 \quad \text{... (4)}$$

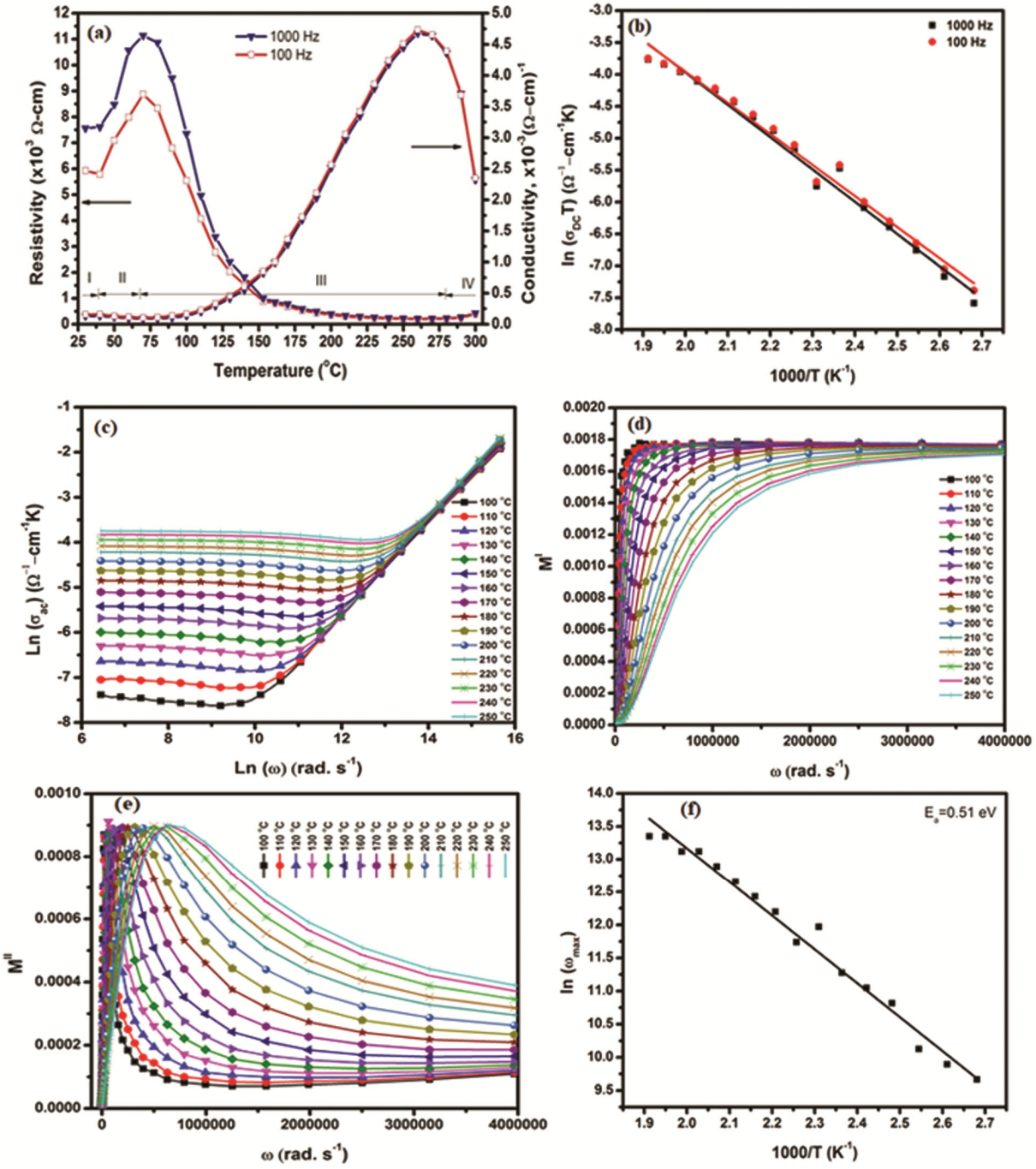

Fig. 2 — (a) Variations of resistivity and conductivity for the ZnO device as function of temperatures with two frequencies 100 and 1000 Hz, (b) ln $(\sigma_{DC}T)$ versus 1000/T for ZnO device, (c) ln (σ_{dc}) versus ln (ω) plots for ZnO device (d) Frequency depedence of the real part of the electric modulus for ZnO device, (e) Frequency depedence of the imaginary part of the electric modulus for the ZnO device, (f) Variation of relaxation frequency (ω_{max}) versus 1000/T for ZnO device

where, σ_{dc} is the DC conductivity, A is a temperature dependent parameter and s a fractional exponent between 0 and 1. Fig. 2c shows the ln (σ_{dc}) versus ln (ω) plot for the ZnO film as function of temperature. The second term in above equation represents the a.c. or polarization conductivity. This power law has been widely observed in many disordered materials like ionically conducting glasses[14], ferroelectric materials[15], semiconductor materials[16], etc., and the behavior is generally related to the mechanism of

charge transport as well as many-body interaction among of charge carriers[17].

Electrical modulus of ZnO device

Elecric modulus formation is an important theory[18], which permits to study charge transport processes in ion conductors and eliminates electrode polarization effect. The electric modulus (M^*) is calculated from the following equation:

$$M^*(\omega) = M' + jM'' \quad \ldots (5)$$

where, $M'=\omega C_0 Z'$ and $M''= \omega C_0 Z'$. Figs 2d and 2e shows the frequency depedence of the (real and imaginary part) of the electric modulus at different tempertures. The plots show an asymmetric behavior with respect to peak maxima which move to higher frequencies with increasing temperature. These spectra also reflect the motions of the ions in the material by exhibiting two apparent relaxation regions. The peak maxima become narrow and appeared to shift toward high frequency region with increasing temperature owing to the distribution of relaxation times in the ZnO film.

The general method to check nature of the dilectric relaxation in the solid is to fit the measured data Kohlrausch-Williams-Watts (KWW) decay function[19]. This function accounts for an asymmetric distribution of relaxation times resulting from a dielectric modulus for differnet tempertures with an approximate frequency representaion of KWW function[20] and allowing a more direct and easy analysis in the frequency domain through the relation.

$$M'' = \frac{M''\max}{1-\beta+\left[(\beta/(1+\beta))\left(\beta(\omega_{\max}/\omega)+(\omega/\omega_{\max})^{\beta}\right)\right]} \quad \ldots (6)$$

where, M_{max} and ω_{max} are the maximum and peak frequency of imaginary part of the modulus. As shown in Fig. 2e, the experimental data are well fitted to above equation and the parameters M_{max}, ω_{max} and β were extracted from the analysis. The β value obtained lies in the range 0.8-1. The frequency region below peak maximum M'', the carriers are confined to potential wells, being mobile on short distances. The frequency ω_{max} (corresponding to M''_{max}) gives the relaxation time τ from the condition $\omega_{max}\tau = 1$. Fig. 2f shows the variation of relaxation frequency, $\omega_{max}(=1/\tau_p)$ versus (1000/T) for ZnO device. The plot obeys the Arrhenius nature and the activation energy calculated from linear regression is found to be 0.51 eV. This value is comparable to activation energy deduced from the impedance semicircles which suggest that the charge carriers have has to overcome the same energy barrier while conducting as well as relaxing.

Ammonia gas sensing properties of ZnO device

Sensor measurement setup

The complex impedance measurements, a Frequency Response, Solartron, Model 1360 coupled with the Solartron Dielectric Interface, 1296 impedance analyzer in the frequency range from 100 Hz to 1 MHz with 100 mV ac signal amplitudes. The impedance spectroscopy unit controlled by a PC was used for data acquisition. A fully automated experimental setup was employed for performing gas sensing tests (Fig. 3a). A temperature controlled furnace was used to heat the dark cylindrical chamber with a volume of 3052 cm^3. The studies were performed at operating temperature fixed at 175°C for all samples. Before measuring the impedance of different materials, the following procedure was applied. First the samples were dried and stabilized by heating at 175°C in vacuum (10^{-5} mbar) for 2 h. Afterwards, the vacuum line was closed and dry synthetic air (80% N_2, 20% O_2) was blown through the chamber atmospheric pressure for some additional 30 min. The different concentrations of gas used were 50, 250 and 500 ppm, respectively. Before starting a sensor measurement, the system was thermally stabilized for 30 min at the desired temperature. The desired concentration of test gas was obtained from calibrated gas bottles by means of volume flow controllers. The conductance of sensors in the presence and absence of ammonia was measured by a Frequency Response, Solartron, Model 1360 coupled with the Solartron Dielectric Interface, 1296.

Stabilization of sensor resistance

When semiconductor materials are used as gas sensors they have either deposited as thin films or thick films or sintered powder. There are two stages of gas sensing effect.

- Atmospheric oxygen gets adsorbed on the surface and removing a carrier from the conduction band of n-type semiconductor gas sensors, becomes O^{-2} or O^- species. This phenomenon reduces the overall conductance.
- The reducing agents, such as hydrogen, carbon monoxide, ammonia and hydrocarbon gases will react with chemiadsorbed oxygen. This process

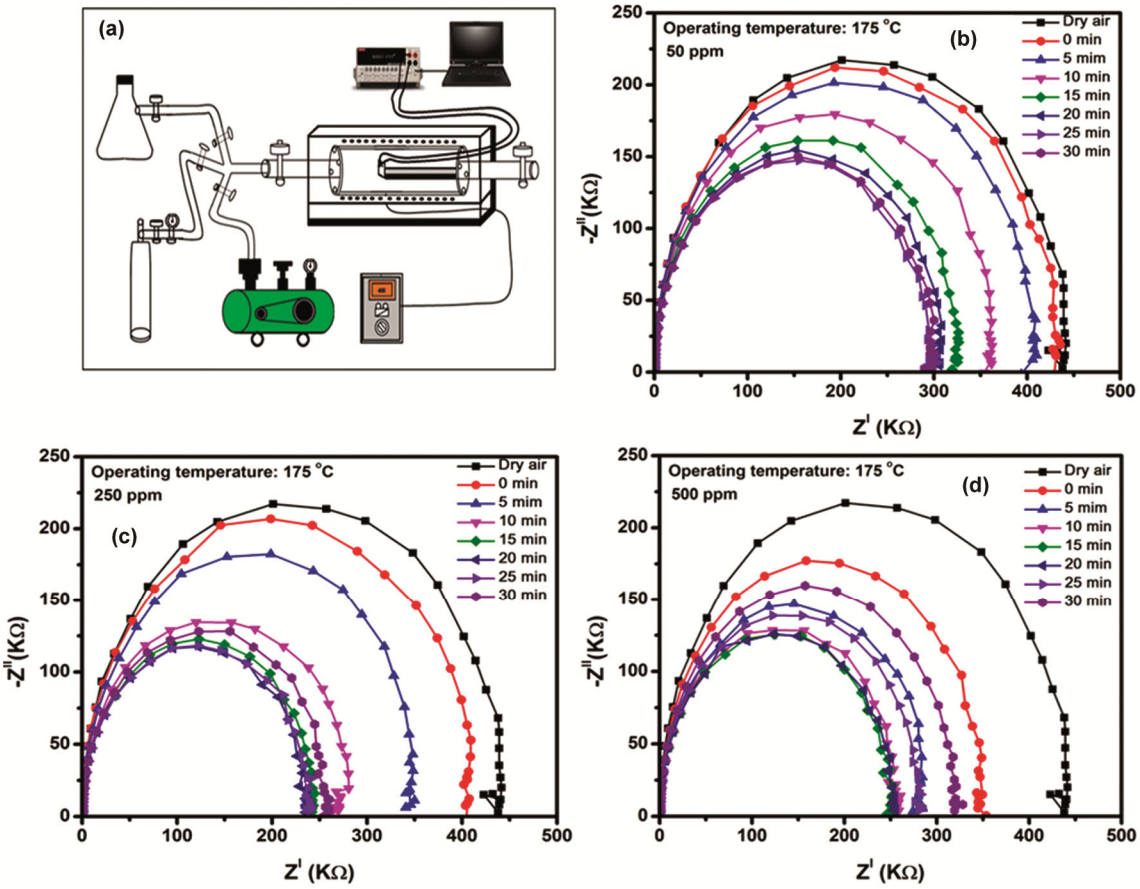

Fig. 3 — (a) Sensor experimental setup-Schematic diagram, (b) Complex impedance of ZnO sensor at 175°C exposed to 50 ppm ammonia, (c) Complex impedance of ZnO sensor at 175°C exposed to 250 ppm ammonia (d) Complex impedance of ZnO sensor at 175°C exposed to 500 ppm ammonia

will reinject the carrier and increase the sensor conductance.

For n-type semiconductors such as ZnO and SnO_2, the concentration of electrons available for conduction can be changed by either an oxidation or reduction process[21]. The resistance of the ZnO sensor must be increased by exposure to oxidizing gas. When the ZnO sensor surface is placed at operating temperature in air ambient, the adsorption of atmospheric surfaces and the oxygen takes place on film surfaces and grain-boundary surfaces and the oxygen accepts electrons to become O_2^-, O^-, or O^{2-} ions, thus decreasing the concentration of the number of charge carriers near the surface giving rise to a depletion region. When exposed to reducing gas like ammonia and ethanol vapour, mutual interaction between the reactant results in oxidation of reducing gas at the surface[22]. This oxidation phenomenon helps in the removal of oxygen ion from ZnO surface resulting in decrease in the barrier height, thus increasing the conductance. During the chemisorption at operating temperature 175°C, oxygen is adsorbed in ionic form as shown in the following reactions[23]

$$O_2 + e^- = O_2^- \quad \text{... (7)}$$

$$O_2^- + e^- = 2O^- \quad \text{... (8)}$$

Above 200°C, the reactivity of O^{-2} species is high[17]. The formation of O^{-2} species is also possible as follows

$$O_2^- + e^- = O^{-2} \quad \text{... (9)}$$

O^{-2} ions are not adsorbed because these species are not stable and are usually trapped by oxygen vacancies. The surface reaction processes can explain the selective ammonia response of the sensor at operating temperature (175°C). Upon exposure to ammonia, a remarkable decrease in the resistance of the sensor was observed[24]. Oxidation of ammonia on the surface of metal oxides can follow more than one

possible route, so several competitive processes may take place at the same time. At least three main reactions for ammonia oxidation have been proposed in the field of gas sensors[25].

$$2NH_{3(g)} + 3O^{-(ads)} \rightarrow N_2 + 3H_2O + 3e^- \quad \text{... (10)}$$

$$2NH_{3(g)} + 5O^{-(ads)} \rightarrow 2NO + 3H_2O + 5e^- \quad \text{... (11)}$$

$$2NH_{3(g)} + 4O^{-(ads)} \rightarrow N_2O + 3H_2O + 5e^- \quad \text{... (12)}$$

where, O^- represents a negatively chemisorbed oxygen species and e^- are free electrons. Other oxygen chemisorbed species or lattice oxygen, could participate in NH_3 oxidation. These reactions just describe the whole process and different intermediate species are likely to appear. The unsatisfactory dynamic behavior exhibited by pure ZnO in NH_3 detection has described for TiO_2 and In_2O_3 based gas sensors[26]. Already it was attributed to the predominance of reaction (11), which leads to the combustion of ammonia into NO. Although ZnO has shown a rather low sensor response to NO in an inert atmosphere[27], it is very well known that NO can be easily transformed into NO_2 in the presence of oxygen, and so it often called NO_x. ZnO is very sensitive to this gas, which makes the resistance increase. Therefore, when NH_3 is introduced, sensor resistance decreases as oxygen is consumed. However, if NO_x are produced, this gas may trap electrons, form NO_x^- species and thus, resistance would increase. This would explain why at higher temperatures there is an abrupt decrease of resistance, followed by a slow increase when NH_3 is introduced, as reaction (12) is specially promoted at high temperature[28]. On the other hand, when NH_3 is removed, oxygen is quickly adsorbed on the surface, which makes sensor resistance increase.

However, NO_x^- is hard to be desorbed, especially at low temperatures. This would explain evershooting problems on the resistance after NH_3 removal, as it has a higher value than before NH_3 introduction and a very slow recovery. To sum up, sensor response of pure ZnO to NH_3 is not completely satisfactory probably due to the interference of NO_x, so selective oxidation of NH_3 is needed in order to improve sensor response. As a matter of fact, N_2 is an inert gas and it has been reported that oxides have a low sensor response to N_2O gas[29].

Time effect

According to the previous results, the working temperature was fixed at 175°C. The effect of time on the Nyquist of the ZnO sensors with ammonia concentrations 50, 250 and 500 ppm is shown in Figs 3b, 3c,3d, respectively, where a single semicircle with a centre on the x-axis was observed. The single arc behaviour was observed by several authors for different metal oxide materials with grains of nano scale dimensions which results in a very narrow relaxation time distribution[30,31]. This behaviour led to a distinguished single relaxation time τ, that could be estimated from the maximum height of the impedance arc where $\tau\omega_{max}=RC\omega_{max}=1$.

It is believed that the mechanism is due to a charge transfer process in the material[32]. The characteristics showed that the diameter of the semicircles decreases in the pressure of 50 ppm of ammonia gas, and it decreased further as the time was increased. It is clear from the Fig. 3b that the semicircles decrease linearly up to 20 min of time, after that slightly increased and the same case is obtained from 250 ppm, 500 ppm exposure to ammonia gas (Figs 3c and 3d). The estimated values of grain boundary resistance and capacitance (R_{gb} and C_{bg}) are presented in Table 1. Since there was no significant change in the values of

Table 1 — Complex impedance analysis of ZnO sensor calculated at different time intervals

Time (min)	50 ppm		250 ppm		500 ppm	
	R_{gb} (kΩ	C_{gb} (pF)	R_{gb} (kΩ)	C_{gb} (pf)	R_{gb} (kΩ)	C_{gb} (pF)
Dry air	864.63	29.17	864.63	29.17	864.63	29.17
During	858.15	29.39	808.84	31.18	707.20	35.66
5	787.42	32.03	700.19	36.02	548.51	36.52
10	708.48	35.60	526.21	30.24	513.82	38.99
15	639.03	39.47	478.96	33.22	491.97	32.35
20	597.80	33.51	477.42	33.33	504.01	31.57
25	608.60	32.92	471.67	33.74	552.33	28.81
30	579.40	34.58	508.54	31.29	656.42	24.24

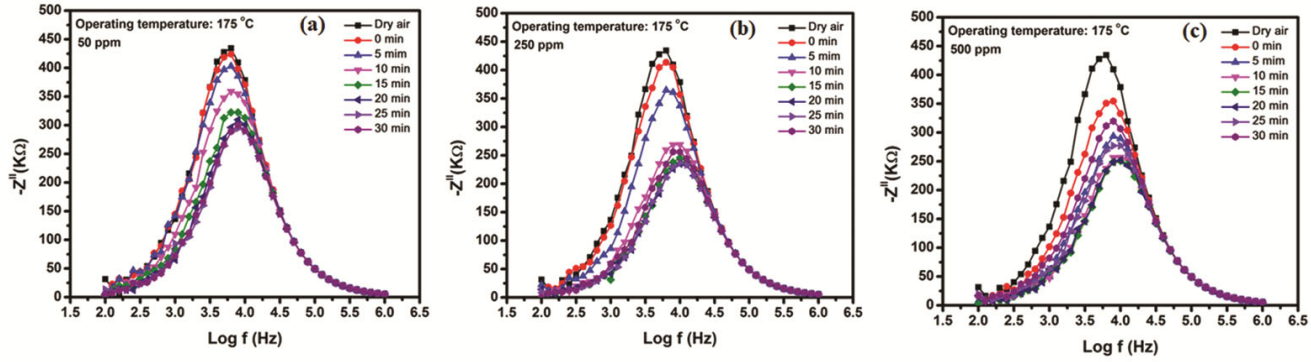

Fig. 4 — Imaginary part of the impedance versus frequency for ZnO sensor under different time intervals exposed to (a) 50 ppm ammonia, (b) 250 ppm ammonia, (c) 500 ppm ammonia

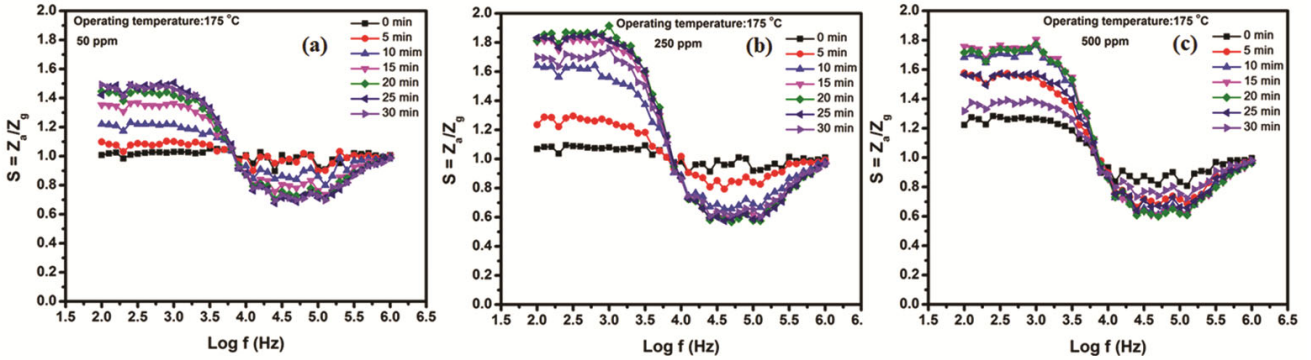

Fig. 5 — Sensitivity of the ZnO sensor at 175°C exposed to (a) 50 ppm ammonia (b) 250 ppm ammonia (c) 500 ppm ammonia

the capacitance, it can be suggested that the ammonia gas mainly affect the surface charge transfer in the grains of ZnO device. The peak frequencies associated with the relaxation process of the impedance were also estimated by repotting the data of imaginary part of the impedance ($-Z''$) against the logarithm of the frequency (Figs 4a, 4b and 4c), where the peaks of the imaginary part of the impedance corresponds to the top of the relaxation semicircles are in accordance with the in Figs 3b, 3b and 3c. It is observed that the peak frequency shifts towards higher frequencies, and the peak height decreases with the increase of exposure time and the ammonia concentrations. The peak broadening suggests the dependence of the relaxation process on the gas concentration[33].

The sensitivity (S) of the prepared ZnO films was evaluated as a function of frequency and ammonia concentration with exposure different time using following relationship;

$$S = \frac{Z_a}{Z_g} \quad \ldots (13)$$

where, Z_a is the real part of the impedance for dry air and Z_g is the real part of the impedance for ammonia atmosphere. Figs 5a, 5b and 5c show the effect of the frequency and ammonia concentrations at an operating temperature 175°C on the sensitivity of the ZnO device. It can be observed that the sensitivity of the sensor remains constant within the frequency range 100 Hz-1 MHz, which is the range where the space charge transfer rules the conductivity process. The sensitivity decreases sharply with the frequency increase and becomes almost constant at a frequency higher than 100 kHz, in which the conductivity is controlled by the surface charge transfer of the grains. This suggests that the sensor could be tuned to achieve maximum sensitivity by selecting a suitable operating frequency range.

Conclusion

Complex impedance spectroscopy has been used to characterize the semiconducting properties of ZnO devices. The presence of space charge polarization at higher temperature arises only due to the mobility of ions and imperfections in the material. DC conductivity shows typical Arrhenius behaviour when observed as a function of temperature. Modulus

analysis has been carried out to understand the mechanism of electrical transport process which indicates the presence of non-Debye type conductivity relaxation in the material. The activation energy calculated from modulus formalism spectra is consistent with the estimated value from impedance spectra, indicating that the ions have to overcome almost same energy barrier while conducting and relaxing. The small difference in the activation energy calculated from relaxation and conductivity studies suggests that both the process may be attributed to the same type of charge carries. The complex impedance behavior of the pure and ZnO sensors at 175°C with different exposure time and 50, 250 and 500 ppm of ammonia has been studied. The sensor exhibited a decrease in resistance when ammonia was introduced in the test chamber. The effect of different ammonia concentrations on the complex impedance behavior was examined. It is suggested that the ammonia gas sensing property is mainly due to the surface charge in the grains of the ZnO sensors.

Acknowledgements

The authors are thankful to University Grants Commission, UGC-SERO, Hyderabad (India), for financial support under the project (No. MRP-4892/14 (SERO/UGC)).

References

1 Bardeen J, *Phys Rev*, 71 (1947) 717.
2 Shawuti S, Sherwani S R, Can M M & Gulgun M A, *Sci Rep*, 8228 (2020) Please give me pages number.
3 Kashif M, Hashim U, Ali E, Saif A, Ali S M U & Willander M, *Microelectron Int*, 29 (2012) 131.
4 Mohamad A S, Hoettges K F & Hughes M P, IEEE Asia-Pacific Conference on Applied Electromagnetics (APACE), (2014).
5 Ramteke R, Kumari K, Bhattacharya S, Sharma S K, Rahman M R, *Curr App Phys*, 22 (2021) 84.
6 Yilmaz M, Demir K C, Turgut G & Aydogan S, *Philos Mag Lett*, 99 (2019) 243.
7 Tewari S & Bhattacharjee A, *Pramana*, 76 (2011) 153.
8 Guruprasad K, Marappan G, Elangovan S, Jayaraman S V, Bharathi K K & Venugopal G, *Nano Express*, 1 (2020) 030020.
9 Sahay P P & Nath R K, *Sens Actuat B: Chem*, 134 (2008) 654.
10 Fan J W, Zhao H J & Zhang X L, *Appl Mech Mater*, 681 (2014) 173.
11 Norouzzadeh P, Mabhouti K, Golzan M M & Naderali R, *J Mater Sci: Mater Electron*, 31 (2020) 7335.
12 Mohamad A S, Hoettges K F & Hughes M P, 2014 IEEE Asia-Pacific Conference on Applied Electromagnetics (APACE) (2015).
13 Belgacem R B, Chaari M, Brana A F, Garcia B J & Matoussi A, *J Am Ceram Soc*, 100 (2017) 2045.
14 Costa J S, Prestat M, Tribollet B, Lescop B, Rioual S, Holzer L & Thierry D, *Chem Electro Chem*, 7 (2020) 2055
15 Wu J, Jia W, Xu C, Gao D & Sun M, *J Biomed Eng Inform*, 3 (2017) 44.
16 Yumak T, Kuralay F, Muti M, Sinag A, Erdem A & Abaci S, *Colloids Surf B: Biointerfaces*, 86 (2011) 397.
17 Viswanath R & Ramasamy S, *Mater Trans*, 42 (2001) 1647.
18 Balasubramani V, Sureshkumar S, Rao T S & Sridhar T M, *ACS Omega*, 4 (2019) 9976.
19 Minami T, Nanto H & Takata S, *Thin Solid Films*, 124 (1985) 43.
20 Patil D R, Patil L A & Patil P P, *Sens Actuat B: Chem*, 126 (2007) 368.
21 Ben B R, Chaari M, Brana A F, Garcia B J & Matoussi A, *J Am Ceram Soc*, 100 (2017) 2045.
22 Lee J, Hwang J H, Mashek J J, Mason T O, Miller A E & Siegel R W, *J Mater Res*, 10 (1995) 2295.
23 Kanazawa E, Sakai G, Shimanoe K, Kanmura Y, Teraoka Y, Miura N & Yamazoe N, *Sens Actuat B: Chem*, 77 (2001) 72.
24 Younas M, Zou L L, Nadeem M, Naeem-ur-Rehman N R, Wang Z L & Ling F C C, *Phys Chem Chem Phys*, 16 (2014) 16030.
25 Chaari M, Ben Belgacem R & Matoussi A, *J Alloys Comp*, 726 (2017) 49.
26 Kailai W, Wenyu Z & Lai E P C, *J Nanosci Nanotechnol*, 21 (2021) 5207.
27 Li X & Castaneda H, *Int J Spectrosc*, Please give me volume number (2018) 1.
28 Nanto H, Minami T & Takata S, *J Appl Phys*, 60 (1986) 482.
29 Tu Y, Kyle C, Luo H, Zhang D W, Das A, Briscoe J & Krause S, *ACS Sens*, 11 (2020) 3568.
30 Kanaparthi S & Govind S S, *Mater Sci Energy Technol*, 3 (2020) 91.
31 Patil P S, Kawasaki S & Hayakawa Y, *Sens Actuat B: Chem*, 255 (2018) 672.
32 Onkar S G, Nagdeote S B, Wadatkar A S & Kharat P B, *J Phys: Conf Ser*, 1644 (2020) 012060.
33 Waleed-Mahmoud E, Ai-Ghamdi A A, Ai-Heniti S & Ai-Ameer S, *J Alloys Comp*, 491 (2010) 742.